Localization of Calmodulin Binding Sites on the Ryanodine Receptor from Skeletal Muscle by Electron Microscopy

Terence Wagenknecht,* Jon Berkowitz,* Robert Grassucci,* Anthony P. Timerman,‡ and Sidney Fleischer‡

*Wadsworth Center for Laboratories and Research, New York State Department of Health, and School of Public Health, State University of New York at Albany, Albany, New York 12201-0509; and ‡Department of Molecular Biology, Vanderbilt University, Nashville, Tennessee 37235 USA

ABSTRACT Calmodulin (CaM) is a regulator of the calcium release channel (ryanodine receptor) of the sarcoplasmic reticulum of skeletal and cardiac muscle. The locations where CaM binds on the surface of the skeletal muscle ryanodine receptor were determined by electron microscopy. Wheat germ CaM was labeled specifically at Cys-27 with a maleimide derivative of a 1.4-nm-diameter gold cluster, and the gold-cluster-labeled CaM was bound to the purified ryanodine receptor. The complexes were imaged in the frozen-hydrated state by cryoelectron microscopy with no stains or fixatives present. In the micrographs, gold clusters were frequently observed near the corners of the square-shaped images of the ryanodine receptors. In some images, all four corners of the receptor were occupied by gold clusters. Image averaging allowed the site of CaM binding to be determined in two dimensions with an estimated precision of 4 nm. No changes were apparent in the quaternary structure of the ryanodine receptor upon binding CaM to the resolution attained, about 3 nm. Side views of the ryanodine receptor, in which the receptor is oriented approximately perpendicular to the much more frequent fourfold symmetric views, were occasionally observed, and showed that the CaM binding site is most likely on the surface of the receptor that faces the cytoplasm. We conclude that the CaM binding site is at least 10 nm from the transmembrane channel of the receptor and, consequently, that long-range conformational changes are involved in the modulation of the calcium channel activity of the receptor by CaM.

INTRODUCTION

The ryanodine receptor (RyR) of skeletal and cardiac muscle has been identified as the sarcoplasmic calcium release channel and a major component of the triad junction, the site of excitation-contraction coupling (for recent reviews see Fleischer and Inui, 1989; McPherson and Campbell, 1993). In skeletal muscle, depolarization of the plasmalemma initiated at the neuromuscular junction causes the RyR to open, thereby releasing Ca^{2+} from the lumen of the sarcoplasmic reticulum into the myoplasm where it triggers contraction. The mechanism of this process remains to be elucidated.

The purified detergent-solubilized RyR is a homotetramer of identical 565-kDa subunits (Imagawa et al., 1987; Inui et al., 1987; Lai et al., 1988; Saito et al., 1989) of known sequence (Takeshima et al., 1989; Zorzato et al., 1990; Otsu et al., 1990). Electron microscopy in conjunction with image processing and three-dimensional reconstruction has shown that the RyR is fourfold symmetric and has a complex internal network of solvent-accessible channels and cavities (Saito et al., 1988; Wagenknecht et al., 1989; Radermacher

et al., 1992, 1994). Morphologically, the isolated RyR appears identical to the foot structures that have been observed in electron micrographs of skeletal muscle (Franzini-Armstrong, 1980; Franzini-Armstrong and Nunzi, 1983; Saito et al., 1989). The foot structures appear to bridge the gap between the sarcoplasmic reticulum and the transverse tubules (invaginations of the plasma membrane) at the triad junctions. The RyR apparently plays a central role in the signaling events that occur during excitation-contraction coupling.

Characterization of the interactions of the RyR with other structural and regulatory proteins of the triad junction is essential to understanding the signal transduction process. We are using cryoelectron microscopy in conjunction with computer image processing as a tool for mapping the binding locations of RyR ligands and for detecting structural changes that might result from such binding. One such ligand modulator, the subject of this report, is CaM.

Equilibrium affinity constants in the nanomolar range have been measured for the binding of CaM to the RyR (Seiler et al., 1984; Yang et al., 1994), and evidence that this interaction itself, without the involvement of CaM-dependent kinases, inhibits calcium release activity has been described (Meissner, 1986; Meissner and Henderson, 1987; Smith et al., 1989). Three potential CaM binding sites have been identified in the sequences of the skeletal and cardiac muscle RyR (Zorzato et al., 1990; Otsu et al., 1990). In skeletal muscle the three regions are clustered between residues 2807 and 3049, a region of the sequence thought to contribute to the large cytoplasmic domain of the receptor. This region is distant in the sequence from the transmembrane, channel-forming region, predicted to lie in the carboxyl-terminal fifth

of the sequence between residues 3978 and 4932 (Zorzato et al., 1990; Takeshima et al., 1989). Potential phosphorylation sites for CaM-dependent protein kinase have also been identified in the RyR sequence and, although CaM-dependent phosphorylation of the RyR has been demonstrated, the physiological effects of phosphorylation remain to be clarified (Chu et al., 1990; Witcher et al., 1991; Wang and Best, 1992; Suko et al., 1993; Herrmann-Frank and Varsanyi, 1993; Hain et al., 1994).

In this study, we show that CaM binds to solubilized, purified RyR and that the site of binding is near the periphery of the cytoplasmic portion of the receptor complex, distant from the transmembrane part of the channel complex.

MATERIALS AND METHODS

Materials

3-(N-maleimidylpropionyl)biocytin (MPB) was from Molecular Probes (Eugene, OR), monomaleimido NANOGOLD (Au$_{1.4-nm}$) was from Nanoprobes, Inc. (Stony Brook, NY), and colloidal gold (5-nm diameter) conjugated to streptavidin (Au$_{5-nm}$-SA) was from Amersham (Buckinghamshire, U.K.). Reagents and materials used for electrophoresis were from BioRad (Cambridge, MA), except for silver enhancement reagents used to detect Au$_{1.4-nm}$-conjugated proteins, which were from Nanoprobes. Wheat germ and biochemicals were from Sigma Chemical Co. (St. Louis, MO).

Isolation of ryanodine receptor and CaM

Rabbit skeletal muscle RyR was purified from membrane fractions derived from the terminal cisternae of sarcoplasmic reticulum by ultracentrifugation through a sucrose gradient as described by Lai et al. (1988) and modified by Timerman et al. (1993). The pooled gradient fractions containing RyR were concentrated by ultrafiltration (Centricon 30; Amicon, Beverly, MA) to about 1 mg/ml. The purified material was obtained in a buffer (buffer A) consisting of 2 mM potassium phosphate (pH 7.2), 0.5 M KCl, 2 mM DTT, 1% CHAPS, and 17–20% sucrose.

CaM was purified from wheat germ by a modification (Strasburg et al., 1988) of the procedure of Yoshida et al. (1983). The purified material was dialyzed versus buffer B (20 mM Tris-HCl (pH 7.4), 0.15 M KCl, 0.1 mM CaCl$_2$) and stored at −90°C.

Preparation of Au$_{1.4nm}$-CaM and biotinylated CaM

Wheat germ CaM contains a cysteine residue (Cys-27) that can be specifically linked to sulfhydryl-specific reagents. Two protocols were tried to couple CaM to monomaleimido-Au$_{1.4-nm}$. The first (Method I) was adapted from the procedure of Strasburg et al. (1988) who attached a fluorescent derivative of N-ethyl maleimide to CaM. CaM (1 mg/ml) was incubated at room temperature for 4 h in 25 mM HEPES (pH 7.5), 43 mM dithiothreitol, 1 mM EDTA, 6.0 M guanidine-HCl. The dithiothreitol and guanidine-HCl were removed by gel filtration on a column (0.7 × 7 cm) of Sephadex G-25 equilibrated with 25 mM HEPES (pH 6.5), 0.1 mM CaCl$_2$. The protein-containing fractions were pooled and concentrated sixfold by ultrafiltration (Microcon 10, Amicon), and solid guanidine-HCl was added to a final concentration of 6.0 M. The coupling reaction was initiated by adding 33 µl of this material to 966 µl of solution containing 90 µM Au$_{1.4-nm}$ that had been reconstituted by the addition of 100 µl of 2-propanol and 866 µl of 25 mM HEPES (pH 6.5), 6 M guanidine-HCl. The mixture was incubated with stirring for 4 h at room temperature and then applied to a gel filtration column (1 × 18 cm) containing Cellufine GCL-90 (Amicon) equilibrated with buffer B. Fractions containing both protein and 1.4-nm gold clusters

(as determined spectrophotometrically from the turbidity at 420 nm) were pooled, portioned into aliquots, flash-frozen in liquid N$_2$, and stored at −90°C. The final concentration of protein was 0.2 mg/ml.

The second protocol (Method II) for attaching maleimido probes to Cys-27 was used for labeling with maleiimido-Au$_{1.4-nm}$ and the biotin derivative of N-ethyl maleimide, MPB. Here the procedure for MPB is described; the procedure for maleimido-Au$_{1.4-nm}$ was essentially the same. The procedure was adapted from that described by Kasturi et al. (1993) for labeling CaM with a fluorescent derivative of N-ethyl maleimide. The main difference from Method I is that guanidine-HCl was absent during the reaction with the maleimide. CaM (150 µg in buffer B) was reduced by incubating it overnight at 4°C in the presence of 1 mM dithiothreitol and 6.0 M guanidine-HCl, which was subsequently removed by gel filtration using Sephadex G-25 equilibrated with 10 mM MOPS (pH 7.0), 90 mM KCl, 2 mM EGTA at 4°C. A volume of 20 mM MPB was added to the CaM-containing fractions such that a 10-fold molar excess of the reagent relative to CaM was attained. The reaction mixture was incubated overnight at 4°C followed by dialysis versus 10 mM MOPS (pH 7.0), 90 mM KCl. The product is hereafter referred to as biotin-CaM.

Preparation of CaM-RyR complexes

Complexes of Au$_{1.4-nm}$-CaM and RyR were prepared by adding 0.5 µl of RyR (1 mg/ml, in buffer A) to 20 µl of Au$_{1.4-nm}$-CaM (1 µM, in buffer B). The mixture was incubated at room temperature for 5 min, and grids were immediately prepared for cryoelectron microscopy over a 10–20 min period. Longer incubation times were avoided to maintain the solubility of the RyR at the low levels of detergent present.

Complexes of biotin-CaM and RyR were prepared as for Au$_{1.4-nm}$-CaM except that the concentration of biotin-CaM was 0.1 µM, and after the 5 min incubation with RyR, 1 µl of Au$_{5-nm}$-SA (undiluted suspension from manufacturer) was added before preparing grids for EM. It was not practical to include higher levels of Au$_{5-nm}$-SA because it contained bovine serum albumin (added by the manufacturer), which would interfere with the microscopy.

Electron microscopy

Procedures for cryoelectron microscopy were as described previously (Radermacher et al., 1992), except that nickel or molybdenum 300-mesh grids were used in place of copper grids and a guillotine device that blotted the specimen grids from both sides was used (Cyrklaff et al., 1990). For specimens containing 1.4-nm gold clusters, two micrographs at 60,000× magnification were recorded for each field, the first with the objective lens underfocused by 1.5–2.0 µm and the second at 0.3–0.7 µm underfocus. The second micrograph was used to verify the locations of the Au$_{1.4-nm}$ clusters tentatively identified in the first micrograph (see Results). The electron dose to the specimen was about 15 electrons/Å^2 per micrograph.

For negative staining 3–5 µl of specimen was applied to a glow-discharged, carbon-coated 300-mesh nickel grid for about 30 s. The grid was then rinsed with 6–8 drops of 1% uranyl acetate (pH not adjusted) applied with a Pasteur pipette, and blotted. Minimal dose techniques were not used for negatively stained specimens.

Image processing

Averaging of selected images of the single RyR molecules from micrographs recorded at 1.5 µm underfocus was done using the SPIDER software package (Frank et al., 1981) as described previously (Radermacher et al., 1992). Efforts to form averages of receptors recorded closer to focus (0.4 µm) have thus far not been successful. To avoid bias in alignment of the images caused by the presence of gold clusters, we used as a reference particle an averaged image of RyR without bound gold that was described in our earlier study (Radermacher et al., 1992). All of the averages shown were fourfold-symmetrized. Essentially similar results were obtained when

a randomly selected particle was used as the initial reference. A reference-free alignment method (Penczek et al., 1992) was also successful, but, unlike the averages obtained when a reference image was used, the densities of the 1.4-nm gold clusters were not equivalent at the four symmetrically related positions before fourfold symmetrization: this asymmetry arises because of the partial occupancy of the CaM binding sites (2–3 gold clusters per RyR) and the contribution of the gold clusters themselves to the calculated correlation functions.

Difference maps were formed by subtracting averaged images of RyRs from averages of $Au_{1.4-nm}$-CaM:RyR complexes after application of a scaling procedure in which an additive constant and a multiplicative scaling factor were determined such that the differences between the two averages were minimized.

Other methods

Polyacrylamide gradient (4–20%) gel electrophoresis in the presence of sodium dodecyl sulfate (SDS) was done by the Laemmli (1970) procedure. Protein bands were stained with Coomassie Brilliant Blue or silver (BioRad silver staining kit). Selective staining of $Au_{1.4-nm}$-conjugated proteins was achieved by silver enhancement as described by the manufacturer of the gold clusters (Nanoprobes). Electrophoresis in the absence of SDS was done according to the directions supplied by the manufacturer of the pre-cast gel (BioRad). Electrophoretic blotting and detection of biotinylated proteins from SDS polyacrylamide gels was done according to Towbin et al. (1979) and as described previously (Wagenknecht et al., 1992). Detection of total protein on blots was by staining with colloidal gold (Rohringer and Holden, 1985). Protein concentrations were determined by a Coomassie Blue dye-binding assay (Bradford, 1976). The activity of the purified wheat germ CaM was determined from its activating effect on cAMP phosphodiesterase (Cheung, 1971).

RESULTS

Labeling of CaM with monomaleimido-$Au_{1.4-nm}$ and MPB

Wheat germ CaM has a single Cys residue at position 27 that is available for chemical modification by sulfhydryl-specific reagents (Strasburg et al., 1988). We have coupled this residue to a monomaleimido-derivatized 1.4-nm-diameter gold cluster ($Au_{1.4-nm}$) so that the CaM binding locations on the RyR can be detected in electron micrographs (see Materials and Methods). The gold cluster consists of a 67 atom gold core surrounded by an organic matrix such that the total diameter is 2.7 nm (Hainfeld, 1992; Hainfeld and Furuya, 1992). Thus, the probe should permit localization of the reactive sulfhydryl with a precision of 2 nm.

The labeling of CaM by the gold cluster compound was monitored by SDS-polyacrylamide gel electrophoresis. Fig. 1 A (lanes 1 and 2) shows that the maleimido-$Au_{1.4-nm}$-treated CaM migrates in the gel as a major band of apparent $M_r \approx 20$ kDa and two minor bands of higher M_r. Lanes 3 and 4, loaded with nontreated CaM, show a major band of apparent $M_r \approx 14$ kDa corresponding to CaM (actual M_r 17 kDa) and two minor bands of lower mobility. The band at ≈ 14 kDa is barely visible in the lanes containing the maleimido-$Au_{1.4-nm}$-treated CaM, indicating that labeling of CaM was nearly quantitative. The band at ≈ 20 kDa (lanes 1 and 2) probably corresponds to CaM linked to one $Au_{1.4-nm}$ cluster. The minor bands of higher apparent M_r might arise from species consisting of gold clusters containing more than one maleimido moiety, each linked to a different CaM. A
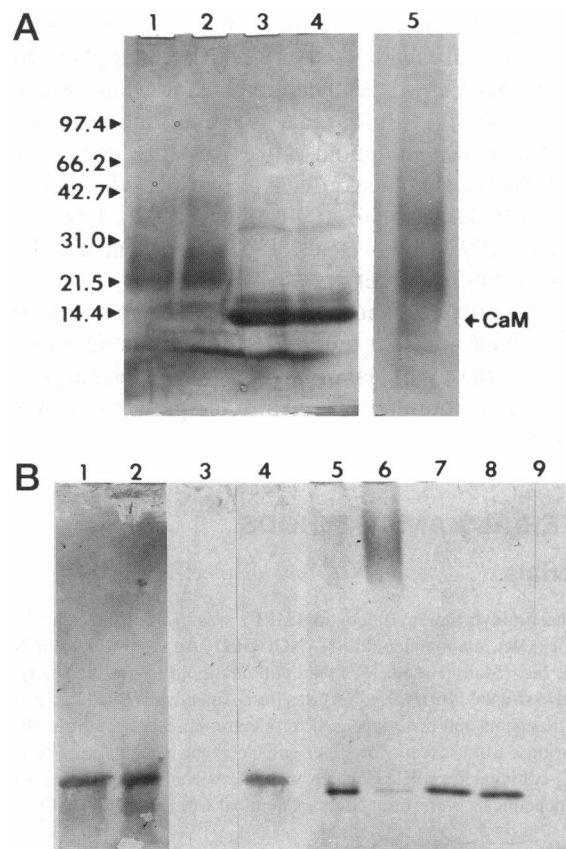

FIGURE 1   Electrophoretic analysis of $Au_{1.4-nm}$-CaM (A) and biotin-CaM (B). (A) SDS-PAGE of $Au_{1.4-nm}$-CaM (prepared by method I, see Materials and Methods). Lanes 1–4 stained with Coomassie Blue followed by silver staining. Lanes 1–4 contain 1 μg of $Au_{1.4-nm}$-CaM, 2 μg of $Au_{1.4-nm}$-CaM, 3 μg of CaM, and 1 μg of CaM, respectively. Lane 5 loaded with 1 μg of $Au_{1.4-nm}$-CaM and silver-enhanced to detect only bands associated with gold clusters (no silver-enhanced bands were visible for lanes loaded with up to 6 μg of CaM, not shown). Arrowheads on left indicate mobility of molecular weight standards (kDa). (B) Lanes 1–4 are from SDS-PAGE and blot transfer to nitrocellulose: lanes 1 and 2 were stained with gold to detect protein and contain 2.5 μg of CaM and 1 μg of MPB-CaM, respectively; lanes 3 and 4 were treated with avidin-alkaline phosphatase to detect biotinylated proteins and contain 2.5 μg of CaM and 1 μg of MPB-CaM, respectively. Lanes 5–9 are from a native (no SDS) gel and were stained with Coomassie blue. Lanes 5 and 6 were loaded with a mixture containing 3 μg of avidin and either 2.5 μg of CaM (lane 5) or 2.5 μg of biotin-CaM (lane 6). Lanes 7–9 contain 2.5 μg each of MPB-treated CaM, CaM, and avidin, respectively. Note that avidin (lane 9) does not stain under these conditions.

similar type of heterogeneity has been observed for other $Au_{1.4-nm}$-protein conjugates (Wilkens and Capaldi, 1992; Braig et al., 1993).

Bands corresponding to gold cluster-labeled peptides can be selectively stained in SDS polyacrylamide gels by silver enhancement as illustrated by Fig. 1 A (lane 5), which shows that the major band detected by staining for total protein (lanes 1 and 2) was indeed coupled to the gold cluster.

The free sulfhydryl on CaM was also coupled to a biotin-maleimide probe (MPB) to confirm some of the results obtained with $Au_{1.4-nm}$-CaM (see below). Biotin-CaM was detected by SDS-PAGE followed by transfer to nitrocellulose and detection of biotinylated species (see Fig. 1 B, lanes 1–4).

The extent of labeling was estimated by "native" polyacrylamide gel electrophoresis (no SDS present) of biotin-CaM to which a stoichiometric amount of avidin had been added (Fig. 1 B, lanes 5–9). Biotinylated CaM in the absence of avidin (lane 7) or nonlabeled CaM in the presence of avidin (lane 5) showed a single band caused by biotin-CaM or CaM (avidin stains much more weakly with Coomassie Blue than CaM and is not visible in lanes 5 and 9). In lane 6, containing biotin-CaM to which avidin had been added, the CaM band is much reduced in intensity and a new broad band appears near the top of the gel. This diffuse band of low mobility is interpreted as biotin-CaM associated with avidin. It appears, on the basis of the decrease in intensity of the band caused by biotin-CaM in lane 6, that the CaM was nearly quantitatively biotinylated.

The activity of the labeled CaMs was determined by an assay that measures the stimulation of phosphodiesterase by Ca^{2+}-CaM (see Materials and Methods). Less than 2% of the activity of unmodified CaM was found for $Au_{1.4-nm}$-CaM prepared by Method I, but full activity was found for $Au_{1.4-nm}$-CaM or biotin-CaM that was prepared by Method II. For unknown reasons, the $Au_{1.4-nm}$-CaM prepared by Method II, despite retaining activity, gave inferior results compared with the material prepared by Method I in the electron microscopy analyses. The main problem with the material prepared by Method II was that many of the gold clusters
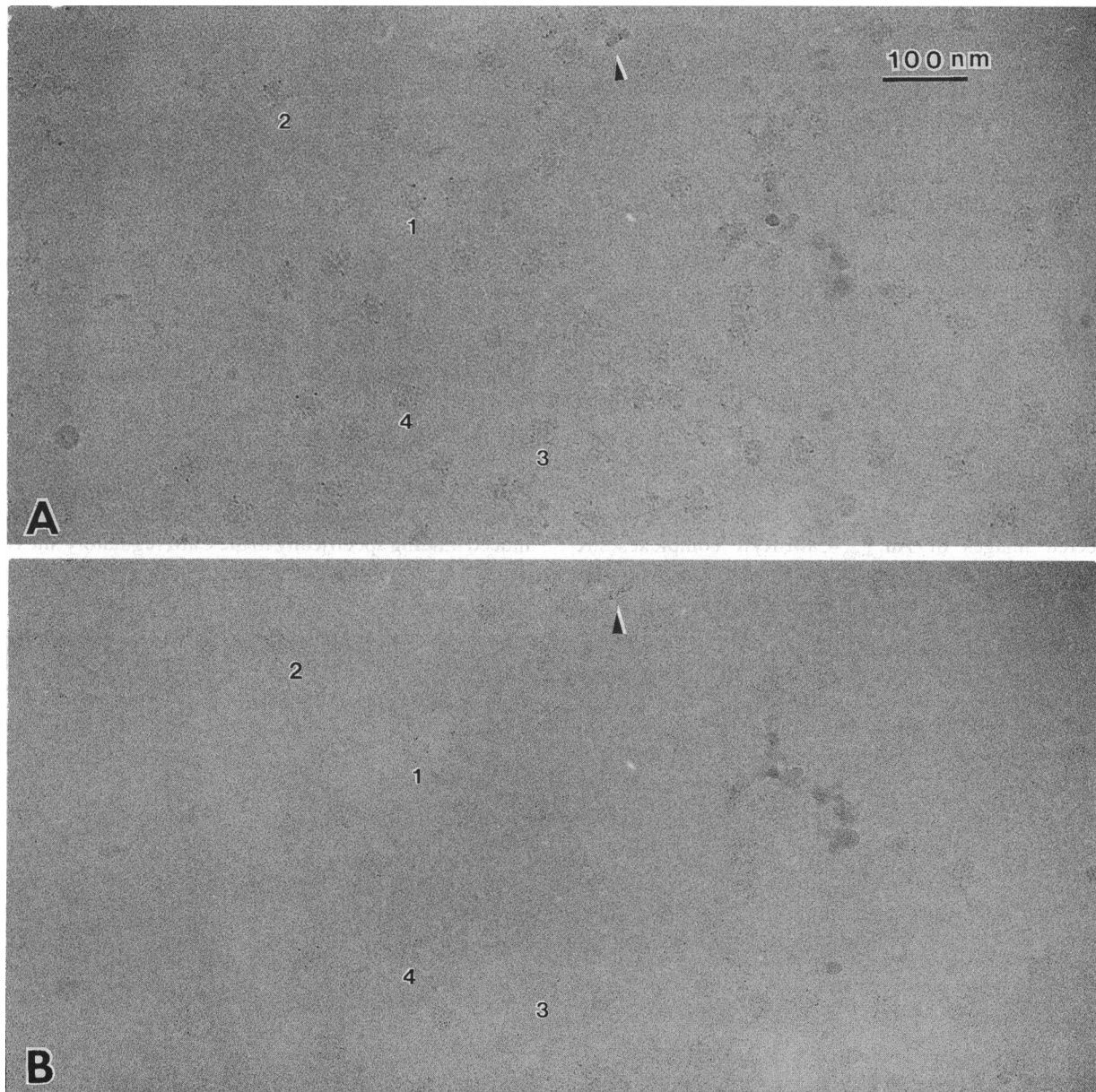

FIGURE 2 Cryoelectron microscopy of frozen-hydrated $Au_{1.4-nm}$-CaM:RyR complexes. A and B show micrographs of identical fields of complexes that were recorded successively with the objective lens underfocused by 1.5 and 0.4 μm. A few of the complexes that contain gold clusters are indicated by numbers in the two micrographs.

appeared to be aggregates of two or more 1.4-nm clusters. Otherwise, the $Au_{1.4-nm}$-CaM prepared by the two methods gave equivalent results. Most of the results from electron microscopy described below were obtained using the $Au_{1.4-nm}$-CaM prepared by method I.

Cryo-EM of $Au_{1.4-nm}$-CaM:RyR complexes

Despite the loss of biological activity in the phosphodiesterase assay, the $Au_{1.4-nm}$-CaM prepared by Method I appeared to bind in a specific manner to solubilized RyR. Fig. 2 shows electron micrographs of frozen-hydrated RyR to which $Au_{1.4-nm}$-CaM had been added. The two electron micrographs shown are of the same field of receptors, the difference between them being that the micrograph in Fig. 2 A was recorded with the objective lens at 1.5 μm underfocus, whereas that in Fig. 2 B was recorded at 0.4 μm underfocus. Low resolution structure is enhanced in the more defocused micrograph, and it is useful for visualizing the RyRs, but the gold clusters are blurred and not always unambiguously identifiable. The closer-to-focus micrograph is more optimal for imaging the gold clusters, but the RyRs are poorly contrasted. We routinely recorded focus pairs of micrographs so that the RyR-associated gold clusters could be positively identified.

From the micrographs in Fig. 2 it is apparent that there are typically from one to four gold clusters present within the boundaries of most RyRs. Most of the RyRs assume orientations on the carbon support film such that their fourfold symmetry axes are perpendicular to the plane of the carbon supporting film, and hence exhibit an overall square shape as has been described previously (Inui et al., 1987; Saito et al., 1988; Lai et al., 1988; Wagenknecht et al., 1989; Radermacher et al., 1992). The gold clusters are, with few exceptions, located near the corners of the RyRs.

Selected images of $Au_{1.4-nm}$-CaM:RyR complexes are shown in Fig. 3, A and B at the two defocus values. From the

images recorded closer to focus (Fig. 3 B), it can be seen that sometimes two or more gold clusters appear bound very close to one another on the RyR (e.g., see second image from left). We do not know whether this reflects multiple, closely spaced binding sites for CaM or some type of artefact involving aggregation of the gold clusters, but we suspect the latter (see image processing results below). Also, shown in Fig. 3 C are a few selected images of $Au_{1.4-nm}$-CaM:RyR complexes in which the $Au_{1.4-nm}$-CaM was prepared by Method II; the images are qualitatively in agreement with those in Fig. 3, A and B, except that more extensive aggregation of the gold clusters was found and the overall level of binding was somewhat reduced.

The following experiments were done to determine whether the the association of the gold clusters with the RyR reflected interactions at the CaM binding sites on the RyR. First, we found that association of $Au_{1.4-nm}$ with RyRs required that the gold clusters be linked to CaM. RyRs treated with a molar excess of inactivated (hydrolyzed) maleimido-$Au_{1.4-nm}$ were associated on average with only 0.1 gold clusters ($N = 50$) as compared with 2.6 clusters per RyR when $Au_{1.4-nm}$-CaM ($N = 165$) was used at the same molar ratio.

As a second test of the binding specificity of $Au_{1.4-nm}$-CaM, we determined whether its binding to the RyR was competitive with unmodified CaM. RyR was incubated with a mixture of $Au_{1.4-nm}$-CaM and CaM (estimated molar ratio 1:4). Cryoelectron microscopy of this mixture and of a specimen prepared under identical conditions, but omitting the unlabeled CaM, showed that the RyR images from the mixture contained an average of 1.0 ($N = 102$) gold cluster, whereas the images from the specimen without CaM contained 2.1 gold clusters ($N = 123$). The difference between these two averages is statistically highly significant ($p < 0.001$) and argues strongly that the $Au_{1.4-nm}$-CaM is indeed binding specifically to the CaM regulatory sites on the RyR. The observed difference in gold cluster occupancy,

FIGURE 3   Selected images from electron micrographs of gold cluster-CaM-treated RyR. (A) Frozen-hydrated $Au_{1.4-nm}$-CaM:RyR complexes prepared using $Au_{1.4-nm}$-CaM prepared by method I (see Materials and Methods). Micrograph recorded with objective lens underfocused by 1.5 μm. (B) Same RyRs as in A except recorded at 0.5 μm underfocus to contrast the gold clusters. (C) Selected images of $Au_{1.4-nm}$-CaM:RyR complexes prepared using $Au_{1.4-nm}$-CaM prepared by method II (see Materials and Methods). Recorded at 1.5 μm underfocus. (D) Negatively stained biotinylated CaM:RyR complexes treated with streptavidin-colloidal gold (5 nm diameter gold). The first three frames show RyRs in fourfold symmetric orientation, and last three show receptors in orientation approximately normal to the fourfold symmetry axis. Underfocus, $\approx$0.5 μm. The width of each frame in A–D is 64 nm. Arrowheads denote positions of gold clusters.
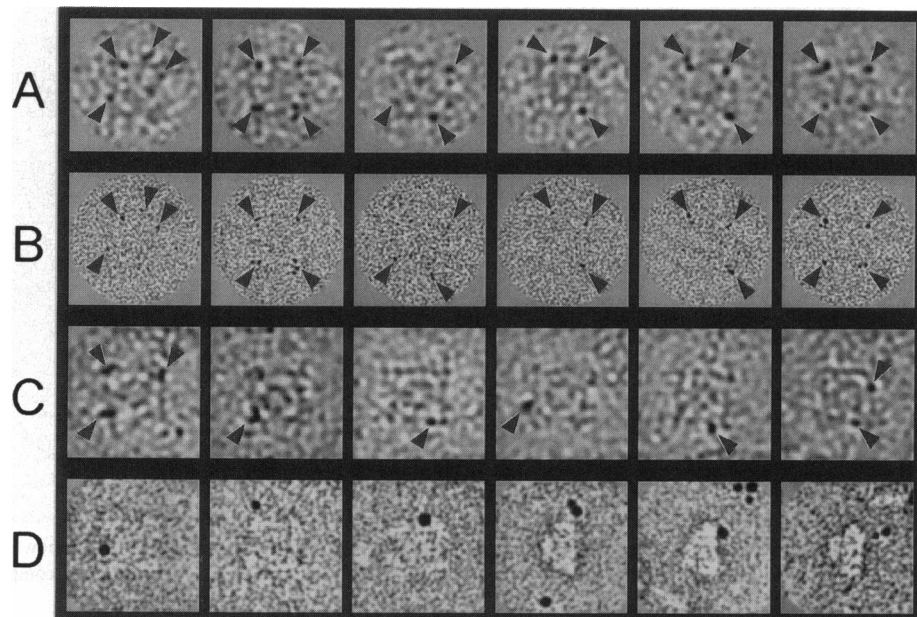
however, is less than expected from the $Au_{1.4-nm}$-CaM:CaM molar ratio. This discrepancy might be caused by an underestimation of this ratio. We have observed that coupling of $Au_{1.4-nm}$ to CaM causes the CaM to stain poorly with Coomassie Blue in electrophoretic gels, and if a similar effect occurs with the Coomassie dye-binding-based protein assay that was used (Bradford, 1976), then the concentration of $Au_{1.4-nm}$-CaM could have been underestimated.

Image processing

To define more precisely the binding sites of $Au_{1.4-nm}$-CaM on the RyR, we selected images of RyRs from the micrograph shown in Fig. 2 *A*, aligned them by correlation methods, and then determined the average of the aligned images (a few of which are shown in Fig. 3 *A*). The criteria used in selecting the images were that the RyR appear structurally intact and that it not be in contact with neighboring particles. Based upon visual inspection of the images, each RyR was associated with two to three gold clusters on average, but the presence of gold clusters was not used as a criterion in selecting images for analysis. To prevent the gold clusters from biasing the alignment procedure, we used as a reference particle a previously determined average of frozen-hydrated RyR obtained in the absence of added $Au_{1.4-nm}$-CaM (Radermacher et al., 1992).

The averaged image obtained from the micrograph of the $Au_{1.4-nm}$-CaM:RyR complexes is shown in Fig. 4 *B* and, for comparison, an average of RyR in the absence of $Au_{1.4-nm}$-CaM is shown in Fig. 4 *A* (an averaged image of RyRs to which nonlabeled CaM had been added (not shown) appeared essentially identical). The major differences between the two averaged images appear as four regions of high density in the average of the $Au_{1.4-nm}$-CaM:RyR specimen (arrowed in Fig. 4 *B*) that are absent in the control average. These symmetrically related regions are located near the corners of the RyR in the same parts of the receptor as that the gold clusters were observed in the original micrographs. The apparent diameter of the high density regions in the averaged image is about twice that of the known diameter of the gold cluster, 1.4 nm. This difference is caused by the effective low-pass filtering imposed by underfocusing the objective lens of the microscope. In micrographs recorded closer to focus (Fig. 3 *B*), the gold clusters indeed appear to be closer to the expected size.

A difference image (Fig. 4 *D*), formed by subtracting the averaged control RyR (Fig. 4 *A*) from the average of $Au_{1.4-nm}$-CaM:RyR (Fig. 4 *B*), also shows these four main regions, along with some minor additional differences distributed throughout the RyR structure. Further study is required to determine whether or not the minor differences are structurally significant, rather than arising from slight differences in defocus, electron dose, or in the thickness of the ice in which the receptors are embedded. Clearly, substantial changes in quaternary structure do not occur when $Au_{1.4-nm}$-CaM binds to the RyR.

Further evidence that the high density regions are caused by gold cluster binding is contained in the variance image

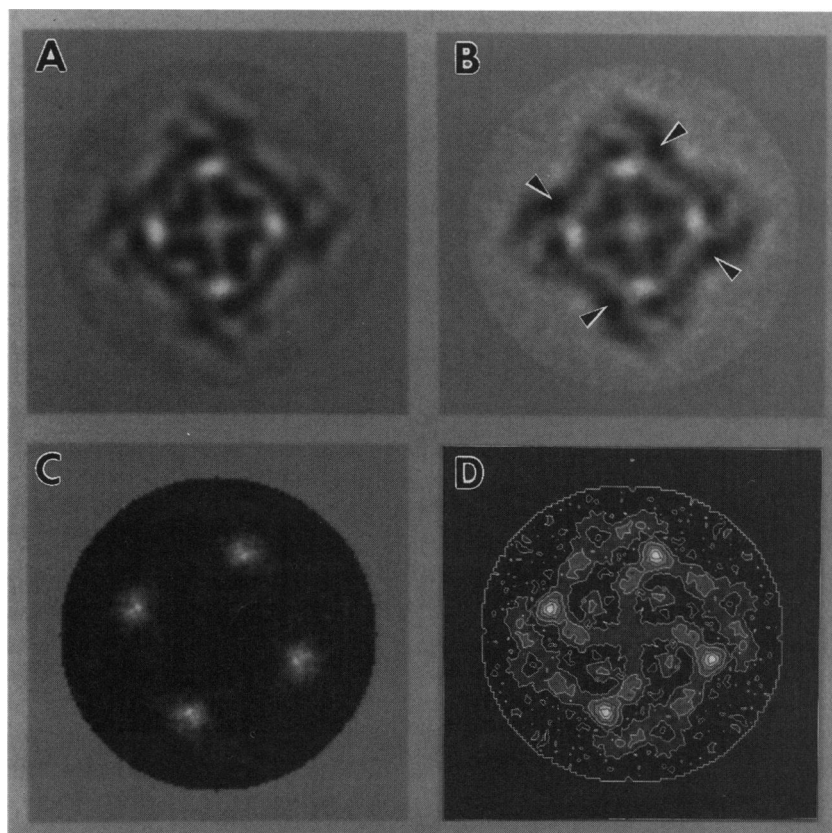FIGURE 4   Image averaging of $Au_{1.4-nm}$-CaM:RyR complexes. (*A*) Averaged image of frozen-hydrated RyR in absence of $Au_{1.4-nm}$-CaM as determined previously by Radermacher et al. (1992). (*B*) Averaged image of RyR that had been incubated with $Au_{1.4-nm}$-CaM determined from images extracted from a micrograph recorded at 1.5 μm underfocus ($N = 89$). Arrowheads denote high density regions attributed to bound $Au_{1.4-nm}$. (*C*) Variance image corresponding to the averaged image in *B*. Highest variance is shown in white. Width of each frame is 64 nm. (*D*) Difference image with superposed contour lines formed by subtracting the average in *A* from that in *B*. The contours are spaced at intervals of 0.025 OD units with the lowest level at -0.025 and the highest at 0.125.

(Fig. 4 C) corresponding to the averaged image of $Au_{1.4-nm}$: RyR (Fig. 4 B). The variance image is a map of the statistical variance associated with each picture element forming the averaged image. This image shows the largest variance (*white* areas) at the same locations as were attributed to the bound gold clusters in the average image. We interpret the high variances as arising because of the partial occupancy of the $Au_{1.4-nm}$-CaM binding locations coupled with the high scattering density of gold clusters relative to protein. The variance image further supports the interpretation that the high density regions arise from the bound gold clusters, as opposed to their arising as the result of a conformational change in the RyR.

From the averaged image $Au_{1.4-nm}$-CaM:RyR, it is possible to determine the positions of the center-of-mass of the density peaks representing the bound gold clusters with much higher precision than the resolution of the average (see Frank et al., 1981). For example, the measured distance between neighboring gold clusters is 16.1 nm with an estimated uncertainty of less than 1 nm. As other structural/functional sites become known, it will be possible to determine their locations relative to one another with similar precision. However, a three-dimensional analysis will be necessary to determine the actual distance between sites in the RyR.

The highly localized nature of the bound gold clusters in Fig. 4 B indicates that the $Au_{1.4-nm}$-CaM did indeed bind principally to four distinct sites related by fourfold symmetry. This finding was not obvious from visual study of the individual images (e.g., those in Fig. 3, A and B), which showed some heterogeneity in the apparent mode of binding. For example, sometimes several gold clusters appeared bound at or near a single site, and the binding locations showed small deviations from the sites revealed by the averaged image.

Conventional EM of biotin-CaM:RyR complexes

Finally, we investigated the binding location of biotin-CaM on the RyR. Biotin-CaM:RyR complexes were detected by the addition of a 5-nm colloidal gold-streptavidin conjugate to the reaction mixture, followed by electron microscopy using the negative stain technique. One of the drawbacks of this labeling strategy is that the precision of localization (≈ 8 nm) is expected to be poorer than that attainable with $Au_{1.4-nm}$ (2 nm). Some typical images in which a colloidal gold cluster is apparently bound to the biotin-CaM:RyR are shown in Fig. 3 E. The gold cluster in these images was most frequently located at the periphery of the RyR, sometimes several nanometers from the outermost boundary of the RyR. Less frequently, the gold cluster was located within the molecular outline of the RyR, but rarely was it near the center of the receptor. Assuming that the variable position of the colloidal gold probe on the RyR was caused by flexibility in its linkage to the biotin-CaM, which binds at a single site, the range of positions is

consistent with a binding location near the corner of the RyR, in agreement with the results obtained with the $Au_{1.4-nm}$-CaM.

Although the precision and reliability with which the CaM binding location on the RyR could be determined were much inferior when biotin-streptavidin-Au_{5-nm} was used as compared with the $Au_{1.4-nm}$-CaM probe (see Discussion), the electron micrographs obtained with this label contained images of RyRs in an orientation that was rarely observed in the micrographs of the frozen-hydrated $Au_{1.4-nm}$-CaM:RyR (rightmost three images in Fig. 3 D). This orientation is approximately perpendicular to the more commonly observed fourfold symmetric views and has been described previously (Saito et al., 1988). In most of these images, the 5 nm gold cluster appeared to be bound to the flatter face of the RyR, opposite to the edge containing the protruding "platform" feature that is thought to contain the transmembrane portion of the RyR (Wagenknecht et al., 1989; Block et al., 1988). Confirmation that CaM binds on this face has come from the observation of a few side views in micrographs of the frozen-hydrated $Au_{1.4-nm}$-CaM:RyR complexes; one such image is marked with an arrowhead in Fig. 2 A.

DISCUSSION

In this study we have shown that CaM, labeled with an electron-dense 1.4-nm-diameter gold cluster, binds in a specific manner to solubilized, purified RyR. Up to four gold clusters can bind per RyR, a homotetrameric complex. This stoichiometry agrees with the number of high affinity CaM sites estimated from binding studies conducted on vesicles derived from sarcoplasmic reticulum (Yang et al., 1994). Cryoelectron microscopy of $Au_{1.4-nm}$-CaM:RyR complexes has shown that the gold clusters are located near the corners of the receptor complexes as viewed in the fourfold symmetric orientation. Observations from side views of the RyR indicate that the CaM-linked gold clusters bind on the cytoplasmic part of the receptor on the surface opposite that containing the transmembrane domain. In Fig. 5 we show where the gold cluster sites would lie on the surface of our recently reported three-dimensional reconstruction of the frozen-hydrated RyR (Radermacher et al., 1994). The four symmetrically related gold cluster sites (*asterisks* in Fig. 5) appear to lie in clefts on the surface of the RyR.

Methodology

The $Au_{1.4-nm}$-probe used in this study has become available recently (Hainfeld and Furuya, 1992; Hainfeld, 1992) and has significant advantages over the more commonly used colloidal gold probes. It can be derivatized with protein-reactive groups, such as the maleimido moiety used in this study and therefore can be directly linked to a macromolecular substrate in a specific manner. This chemical specificity, together with the small size of the $Au_{1.4-nm}$ cluster,
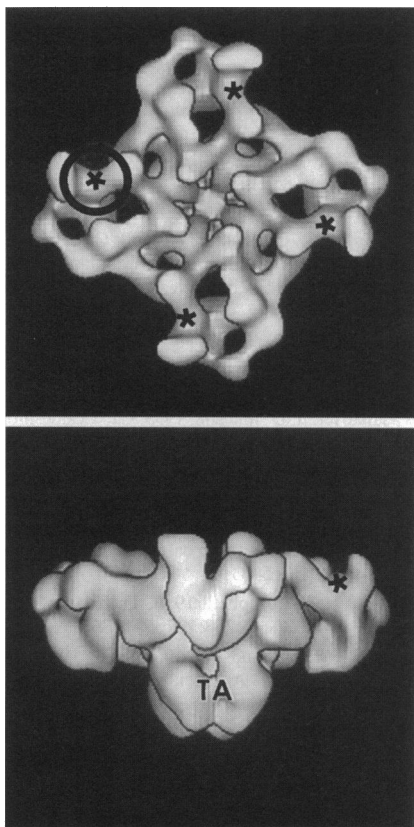
FIGURE 5 Locations of bound $Au_{1.4-nm}$-CaM in three dimensions. The positions of the bound gold clusters were inferred by projecting their locations in the two-dimensional averaged $Au_{1.4-nm}$-CaM:RyR complex (Fig.4 B) onto the cytoplasmic face of the three-dimensional reconstruction of frozen-hydrated RyR reported by Radermacher et al. (1994). The top image shows the RyRs cytoplasmic face viewed parallel to the fourfold symmetry axis. The gold cluster locations are indicated by asterisks; one of the sites is centered within a circle of radius equal to 4 nm to indicate the area within which the center-of-mass of the CaM must lie (see Discussion). The bottom image shows a side view of the RyR (i.e., a view perpendicular to the fourfold symmetry axis) with one of the gold cluster locations denoted by an asterisk. TA, transmembrane assembly.

means that the clusters observed in micrographs of macromolecules labeled this compound should lie within 2 nanometers of their respective reactive sulfhydryls. In contrast, colloidal gold probes are usually attached to the macromolecule of interest via an intermediary protein, such as an Fab fragment or streptavidin, which reduces the accuracy of localization achievable to ≈ 8 nm or more.

Another superior property of $Au_{1.4-nm}$ probes is the reported low affinity of the $Au_{1.4-nm}$ itself for proteins (Hainfeld and Furuya, 1992), which was confirmed in this study. In contrast, the streptavidin-colloidal gold probe that we used to detect biotin-CaM bound to RyRs in electron micrographs showed levels of nonspecific binding many times higher than was found for $Au_{1.4-nm}$-CaM and, consequently, it was difficult to distinguish confidently between specific and nonspecific gold-RyR complexes.

To realize the degree of precision permitted by the $Au_{1.4-nm}$-probe, we chose to image the gold-cluster-labeled com-

plexes in the frozen-hydrated state. There is general agreement that macromolecular ultrastructure is better preserved in this state than in dehydrated, negatively stained, or freeze-dried specimens (Dubochet et al., 1988; Chiu, 1993). When we examined $Au_{1.4-nm}$:RyR complexes in the presence of negative stains (data not shown), the superior preservation of frozen-hydrated specimens was immediately apparent; the number of gold clusters bound per RyR was several times less for negatively stained than for frozen-hydrated specimens.

Location of the CaM binding sites on the RyR

Although the position of the $Au_{1.4-nm}$ on the RyR can be determined with nanometer precision from averaged images (Fig. 4), there is considerably more uncertainty about the position of CaM itself. This uncertainty arises because it is the gold cluster that is being detected, not the CaM. Depending on the orientation assumed by the CaM when it binds to the RyR, and the position on the CaM where the gold cluster is attached, the center-of-mass of the CaM could lie up to several nanometers in any direction from the gold cluster. In the worst case, how far might the actual CaM-binding site be from the gold cluster? To answer this question, we consider the three-dimensional structure of CaM.

Atomic models for CaM-peptide complexes in which the bound peptide mimics the binding site for CaM that is found on CaM-regulated proteins have been determined for three different peptides (Ikura et al., 1992; Meador et al., 1992, 1993). The structure of the CaM is similar in these complexes, and so it seems likely that these models apply generally to most, if not all, CaMs bound to their respective target proteins. Cys-27, the residue of yeast CaM that was labeled with $Au_{1.4-nm}$, corresponds to residue 26 in the mammalian CaM-peptide atomic models and, on the basis of the models, it is apparent that the sulfhydryl group of Cys-27 is within 2 nm of the center-of-mass of the bound peptide. Thus, allowing for the additional 2 nm from the gold cluster to the reactive sulfhydryl (see discussion above), CaM binding sites should lie within 4 nm of the centers of the four gold cluster positions present in the averaged image of $Au_{1.4-nm}$-CaM: RyR (Fig. 4 B).

Experiments in vitro have shown that binding of CaM to the RyR affects channel function by biasing channel gating to favor the closed state (Meissner, 1986; Meissner and Henderson, 1987; Smith et al., 1989). The transmembrane ion-conducting channel is thought to be located at or near the center of the RyR when viewed in the fourfold symmetric orientation. In the two-dimensional projection average shown in Fig. 4 B, the centers-of-mass of the regions attributed to the bound gold clusters are 11.4 ± 1 nm from the center of the RyR. The actual distance (i.e., in three dimensions) is probably significantly greater than this because the $Au_{1.4-nm}$-CaM binding locations and the transmembrane domain of the RyR are on opposite faces of the cytoplasmic domain. On the basis of our most recent three-dimensional reconstruction of the frozen-hydrated RyR (Radermacher et al., 1994), we estimate that the distance from the gold clusters to the cytoplasmic

end of the transmembrane ion channel is about 14 nm (see Fig. 5). Thus, allowing for the 4-nm uncertainty in the locations where CaM itself binds relative to the $Au_{1.4-nm}$, it would appear that CaM binds at least 10 nm from the ion-conducting transmembrane channel of the RyR. Clearly, based on the results of this study, CaM does not modulate RyR activity by binding in the transmembrane ion-conducting channel. More likely, binding of CaM induces allosteric, long-range structural changes that influence channel gating.

Having established in this study that CaM can be nearly quantitatively bound and localized on the RyR under the experimental conditions required for cryoelectron microscopy, it should now be feasible to detect RyR-bound CaM directly, without the requirement of a gold cluster label. This should allow the binding site to be localized even more precisely.

REFERENCES

Block, B. A., T. Imagawa, K. P. Campbell, and C. Franzini-Armstrong. 1988. Structural evidence for direct interaction between the molecular components of the transverse tubule/sarcoplasmic reticulum junction in skeletal muscle. *J. Cell Biol.* 107:2587–2600.

Bradford, M. 1976. A rapid and sensitive method for the quantitation of microgram quantities of protein utilizing the principle of protein-dye binding. *Anal. Biochem.* 72:248–254.

Braig, K., M. Simon, F. Furuya, J. F. Hainfeld, and A. L. Horwich. 1993. A polypeptide bound by the chaperonin groEL is localized within a central cavity. *Proc. Natl. Acad. Sci. USA.* 90:3978–3982.

Cheung, W. Y. 1971. Cyclic 3′,5′-nucleotide phosphodiesterase. Evidence for and properties of a protein activator. *J. Biol. Chem.* 246:2859–2869.

Chiu, W. 1993. What does electron cryomicroscopy provide that x-ray crystallography and NMR spectroscopy cannot. *Annu. Rev. Biophys. Biomol. Struct.* 22:233–255.

Chu, A., C. Sumbilla, G. Inesi, S. D. Jay, and K. P. Campbell. 1990. Specific association of calmodulin-dependent protein kinase and related substrates with the junctional sarcoplasmic reticulum of skeletal muscle. *Biochemistry.* 29:5899–5905.

Cyrklaff, M., M. Adrian, and J. Dubochet. 1990. Evaporation during preparation of unsupported thin vitrified aqueous layers for cryo-electron microscopy. *J. Electron Microsc. Tech.* 16:351–355.

Dubochet, J., M. Adrian, J.-J. Chang, J.-C. Homo, J. Lepault, A. W. McDowall, and P. Schultz. 1988. Cryo-electron microscopy of vitrified specimens. *Q. Rev. Biophys.* 21:129–228.

Fleischer, S., and M. Inui. 1989. Biochemistry and biophysics of excitation-contraction coupling. *Annu. Rev. Biophys. Biophys. Chem.* 18:333–364.

Frank, J., B. Shimkin, and H. Dowse. 1981. SPIDER—a modular software system for electron image processing. *Ultramicroscopy.* 6:343–358.

Franzini-Armstrong, C. 1980. Structure of the sarcoplasmic reticulum. *Fed. Proc.* 39:2403–2409.

Franzini-Armstrong, C., and G. Nunzi. 1983. Junctional feet and particles in the triads of a fast-twitch muscle fibre. *J. Muscle Res. Cell Motil.* 4:233–252.

Hain, J., S. Nath, S. Fleischer, and H. Schindler. 1994. Phosphorylation modulates the function of the calcium release channel of sarcoplasmic reticulum from skeletal muscle. *Biophys. J.* In press.

Hainfeld, J. F. 1992. Site-specific cluster labels. *Ultramicroscopy.* 46:135–144.

Hainfeld, J. F., and F. R. Furuya. 1992. A 1.4-nm gold cluster covalently attached to antibodies improves immunolabeling. *J. Histochem. Cytochem.* 40:177–184.

Herrmann-Frank, A., and M. Varsanyi. 1993. Enhancement of Ca^{2+} release channel activity by phosphorylation of the skeletal muscle ryanodine receptor. *FEBS Lett.* 332:237–242.

Ikura, M., G. M. Clore, A. M. Gronenborn, G. Zhu, C. B. Klee, and A. Bax. 1992. Solution structure of a calmodulin-target peptide complex by multidimensional NMR. *Science.* 256:632–638.

Imagawa, T., J. S. Smith, R. Coronado, and K. P. Campbell. 1987. Purified ryanodine receptor from skeletal muscle sarcoplasmic reticulum is the Ca^{2+}-permeable pore of the calcium release channel. *J. Biol. Chem.* 262:16636–16643.

Inui, M., A. Saito, and S. Fleischer. 1987. Purification of the ryanodine receptor and identity with feet structures of junctional terminal cisternae of sarcoplasmic reticulum from fast skeletal muscle. *J. Biol. Chem.* 262:1740–1747.

Kasturi, R., C. Vasulka, and J. D. Johnson. 1993. Ca^{2+}, caldesmon, and myosin light chain kinase exchange with calmodulin. *J. Biol. Chem.* 268:7958–7964.

Laemmli, U. K. 1970. Cleavage of structural proteins during the assembly of the head of bacteriophage T4. *Nature.* 227:680–685.

Lai, F. A., H. P. Erickson, E. Rousseau, Q. Y. Liu, and G. Meissner. 1988. Purification and reconstitution of the calcium release channel from skeletal muscle. *Nature.* 331:315–319.

McPherson, P. S., and K. P. Campbell. 1993. The ryanodine receptor/Ca^{2+} release channel. *J. Biol. Chem.* 268:13765–13768.

Meador, W. E., A. R. Means, and F. A. Quiocho. 1992. Target enzyme recognition by calmodulin: 2.4 Å structure of a calmodulin-peptide complex. *Science.* 257:1251–1255.

Meador, W. E., A. R. Means, and F. A. Quiocho. 1993. Modulation of calmodulin plasticity in molecular recognition on the basis of x-ray structures. *Science.* 262:1718–1721.

Meissner, G. 1986. Evidence of a role for calmodulin in the regulation of calcium release from skeletal muscle sarcoplasmic reticulum. *Biochemistry.* 25:244–251.

Meissner, G., and J. S. Henderson. 1987. Rapid calcium release from cardiac sarcoplasmic reticulum vesicles is dependent on Ca^{2+} and is modulated by Mg^{2+}, adenine nucleotide, and calmodulin. *J. Biol. Chem.* 262:3065–3073.

Otsu, K., H. F. Willard, V. K. Khanna, F. Zorzato, N. M. Green, and D. H. MacLennan. 1990. Molecular cloning of cDNA encoding the Ca^{2+} release channel (ryanodine receptor) of rabbit cardiac muscle sarcoplasmic reticulum. *J. Biol. Chem.* 265:13472–13483.

Penczek, P., M. Radermacher, and J. Frank. 1992. Three-dimensional reconstruction of single particles embedded in ice. *Ultramicroscopy.* 40:33–53.

Radermacher, M., V. Rao, R. Grassucci, J. Frank, A. P. Timerman, S. Fleischer, and T. Wagenknecht. 1994. Cryo-electron microscopy and three-dimensional reconstruction of the calcium release channel/ryanodine receptor from skeletal muscle. *J. Cell Biol.* 127:411–422.

Radermacher, M., T. Wagenknecht, R. Grassucci, J. Frank, M. Inui, C. Chadwick, and S. Fleischer. 1992. Cryo-EM of the native structure of the calcium release channel/ryanodine receptor from sarcoplasmic reticulum. *Biophys. J.* 61:936–940.

Rohringer, R., and D. W. Holden. 1985. Protein blotting: detection of proteins with colloidal gold, and glycoproteins and lectins with biotin-conjugated and enzyme probes. *Anal. Biochem.* 144:118–127.

Saito, A., M. Inui, M. Radermacher, J. Frank, and S. Fleischer. 1988. Ultrastructure of the calcium release channel of sarcoplasmic reticulum. *J. Cell Biol.* 107:211–219.

Saito, A., M. Inui, J. S. Wall, and S. Fleischer. 1989. Mass measurement of the feet structures/calcium release channel of sarcoplasmic reticulum by scanning transmission electron microscopy (STEM). *Biophys. J.* 55:206a. (Abstr.)

Seiler, S., A. D. Wegener, D. D. Whang, D. R. Hathaway, and L. R. Jones. 1984. High molecular weight proteins in cardiac and skeletal muscle junctional sarcoplasmic reticulum vesicles bind calmodulin, are phosphorylated, and are degraded by Ca^{2+}-activated protease. *J. Biol. Chem.* 259:8550–8557.

Smith, J. S., E. Rousseau, and G. Meissner. 1989. Calmodulin modulation of single sarcoplasmic reticulum Ca^{2+}-release channels from cardiac and skeletal muscle. *Circ. Res.* 64:352–359.

Strasburg, G. M., M. Hogan, W. Birmachu, D. D. Thomas, and C. F.

Louis. 1988. Site-specific derivatives of wheat germ calmodulin. Interactions with troponin and sarcoplasmic reticulum. *J. Biol. Chem.* 263:542–548.

Suko, J., I. Maurerfogy, B. Plank, O. Bertel, W. Wyskovsky, M. Hohenegger, and G. Hellmann. 1993. Phosphorylation of Serine-2843 in ryanodine receptor-calcium release channel of skeletal muscle by cAMP-dependent, cGMP-Dependent and CaM-dependent protein kinase. *Biochim. Biophys. Acta.* 1175:193–206.

Takeshima, H., S. Nishimura, T. Matsumoto, H. Ishida, K. Kangawa, N. Minamino, H. Matsuo, M. Ueda, M. Hanaoka, T. Hirose, and S. Numa. 1989. Primary structure and expression from complementary DNA of skeletal muscle ryanodine receptor. *Nature.* 339:439–445.

Timerman, A. P., E. Ogunbumni, E. Freund, G. Wiederrecht, A. R. Marks, and S. Fleischer. 1993. The calcium release channel of sarcoplasmic reticulum is modulated by FK-506-binding protein. Dissociation and reconstitution of FKBP-12 to the calcium release channel of skeletal muscle sarcoplasmic reticulum.. *J. Biol. Chem.* 268:22992–22999.

Towbin, H., T. Staehelin, and J. Gordon. 1979. Electrophoretic transfer of proteins from polyacrylamide gels to nitrocellulose sheets: procedure and some applications. *Proc. Natl. Acad. Sci. USA.* 76:4350–4354.

Wagenknecht, T., R. Grassucci, J. Berkowitz, and C. Forneris. 1992. Configuration of interdomain linkers in pyruvate dehydrogenase complex of *Escherichia coli* as determined by cryoelectron microscopy. *J. Struct. Biol.* 109:70–77.

Wagenknecht, T., R. Grassucci, J. Frank, A. Saito, M. Inui, and S. Fleischer. 1989. Three-dimensional architecture of the calcium channel/foot structure of sarcoplasmic reticulum. *Nature.* 338:167–170.

Wang, J. X ., and P. M. Best. 1992. Inactivation of the sarcoplasmic reticulum calcium channel by protein kinase. *Nature.* 359:739–741.

Wilkens, S., and R. A. Capaldi. 1992. Monomaleimidogold labeling of the gamma-subunit of the Escherichia-coli F(1) ATPase examined by cryo-electron microscopy. *Arch. Biochem. Biophys.* 299:105–109.

Witcher, D. R., R. J. Kovacs, H. Schulman, D. C. Cefali, and L. R. Jones. 1991. Unique phosphorylation site on the cardiac ryanodine receptor regulates calcium channel activity. *J. Biol. Chem.* 266:11144–11152.

Yang, H. C., M. M. Reedy, C. L. Burke, and G. M. Strasburg. 1994. Calmodulin interaction with the skeletal muscle sarcoplasmic reticulum calcium channel protein. *Biochemistry.* 33:518–525.

Yoshida, M., O. Minowa, and K. Yagi. 1983. Divalent cation binding to wheat germ calmodulin. *J. Biochem.* 94:1925–1933.

Zorzato, F., J. Fujii, K. Otsu, M. Phillips, N. M. Green, F. A. Lai, G. Meissner, and D. H. MacLennan. 1990. Molecular cloning of cDNA encoding human and rabbit forms of the Ca^{2+} release channel (ryanodine receptor) of skeletal muscle sarcoplasmic reticulum. *J. Biol. Chem.* 265:2244–2256.